



*Supplement of*

## **Speciated measurement of bicyclic peroxy radicals via iodide-CIMS and its implication on OH-initiated aromatic oxidation**

**Yi Liu et al.**

*Correspondence to:* Xin Li (li\_xin@pku.edu.cn)

The copyright of individual parts of the supplement might differ from the article licence.

## Table of contents

	Table S1. Calibration System: experimental conditions of aromatic-RO <sub>2</sub> calibrations. ....	10
	Table S2. Instrumentations in this study. ....	10
	Table S3. Theoretical sensitivity of Vocus AIM and traditional I-CIMS. ....	10
5	Table S4. Information of aromatics and their tracer products detected by Vocus AIM (I-CIMS).....	11
	Table S5. Information of aromatics and their tracer products detected by Vocus PTR. ....	11
	Table S6. Wall accommodation coefficients and wall loss rates of aromatic precursors and major tracer products. ....	13
	Table S7. Calibration System: branching ratios of different reaction pathways in calibrations. ....	14
	Table S8. Oxidation Flow Reactor: branching ratios of different reaction pathways in toluene oxidation. ....	15
10	Table S9. Oxidation Flow Reactor: branching ratios of different reaction pathways in m-xylene oxidation. ....	15
	Table S10. Measurement uncertainty contributions in tol-BPRs calibration. ....	16
	Table S11. Measurement uncertainty contributions in m-xyl-BPRs calibration. ....	17
	Table S12. Calibration results for Vocus AIM in this study. ....	18
	Table S13. Significance test for the branching ratio of bicyclic pathway by the direct method and the product-yield method at	
15	different precursor concentration. ....	19
	Scheme S1. Chemical mechanism for toluene-OH oxidation. ....	20
	Scheme S2. Chemical mechanism for m-xylene-OH oxidation. ....	21
	Figure S1. Calibration results for Vocus AIM in this study. ....	22
	Figure S2 Relationship between the sensitivities and the corresponding dV <sub>50</sub> values of standards in the AIM-CIMS (left). dV <sub>50</sub> -	
20	based segmented linear fitting of the sensitivity and the product of the square root of m/z and fragmentation ratio (right). ...	22
	Figure S3 Relationship between relative transmission efficiencies of ions and their mass-to-charge ratios (m/z). ....	23
	Figure S4 Comparison of calculated and measured sensitivities for different classes of compounds. ....	23
	Figure S5 Calibration of the sensitivity of HO <sub>2</sub> radical by Vocus AIM. ....	24
	Figure S6 Sampling loss assessment in PFA line (referenced to the signal at a line length of 0.1 m. ....	24
25	Figure S7 Comparison of RO <sub>2</sub> concentration in the calibrated system estimated using two methods in the oxidation of (left)	
	toluene and (right) m-xylene. ....	25
	Figure S8 Temporal evolution of selected species according to the calibration flow tube kinetic model. ....	25
	Figure S9 The fraction of RO <sub>2</sub> radicals according to the calibration flow tube kinetic model. ....	26
	Figure S10 Sensitivity comparison between chosen and proxy-optimal conditions. ....	26

## Section S1. Iodide Chemical Ionization Time-of-Flight Mass Spectrometry with an AIM Reactor (Vocus AIM)

### S1.1 Iodide Adduct Chemical Ionization

Vocus AIM supports various reagent ions of both positive and negative polarity. In this work, we chose iodide ions ( $I^-$ ) as reagent ions.  $I^-$  is known for its remarkable sensitivity toward compounds containing a hydroxy group, which forms an adduct with  $I^-$  through a hydrogen bond, resulting in minimal fragmentation (Lee et al., 2014). Therefore,  $I^-$  has been applied in the measurement of oxidation products containing hydroxyl groups with semi-/low-volatility (He et al., 2024; He et al., 2023; Berndt et al., 2019; Wang et al., 2018; Zhao et al., 2018). Reaction S1 and Reaction S2 imply that compounds with hydroxy groups as M always forms an adduct  $M+127$  with  $I^-$  through a hydrogen bond,



Owing to the lower-energy ionization reaction, the fragmentation of the iodide adduct is limited. This was confirmed by calibration results in our previous work, which showed that  $I^-$ -CIMS exhibited minimal fragmentation for the majority of the examined standards (He et al., 2024; He et al., 2023). Therefore, the fragmentation of  $RO_2$  radicals in this work was not considered, and the iodide adducts of  $RO_2$  radicals were assumed to be detected at  $m/z (M)+127$ . We identified  $C_xH_{2y+1}O_2I^-$  as the type of iodide adduct produced from  $RO_2$  radicals, as they always contain an odd number of hydrogen atoms. And we attributed the observed  $C_7H_9O_5I^-$  signal at  $m/z$  300 solely to the bicyclic peroxide radicals (BPRs) from toluene. Similarly, the BPRs formed from the oxidation of xylene was identified as  $C_8H_{11}O_5I^-$  at  $m/z$  314.

### S1.2 Theoretical Maximum Sensitivity

For adduct ionization, sensitivity toward a certain species is influenced by two main factors: the formation rate of product ions, governed by collision frequency and the available energy in the reactor, and the transmission efficiency of these product ions to the detector, as described in Eq. 1. However, it is difficult to determine the parameters in the equation to obtain the theoretical sensitivity with calibration experiments.

Here, we used Eq. S1 to describe theoretical maximum sensitivity ( $S_{max}$ ) of CIMS (Isaacman-Vanwertz et al., 2018). In the Eq. S1, reagent ions interact with sample gas in IMR and the reaction are assumed to collide at a rate,  $k_{coll}$ , of  $1 \times 10^{-9} \text{ cm}^3 \text{ molecular}^{-1} \text{ s}^{-1}$ :

$$S_{max} = \frac{[M]_{IMR} \times f \times k_{coll} \times t_{IMR}}{10^6} \text{ (ncps/pptv)} \quad (\text{Eq. S1})$$

where  $[M]_{IMR}$  is the total concentration of gas molecules in IMR,  $f$  is the ratio of concentrations of gas molecules in sample to that in IMR, so  $f = 0.88$  in Vocus AIM and  $t_{IMR}$  is the residence time of the IMR.

In Vocus AIM, the reagent ions at a flow rate of 250 sccm were mixed with sample gas at a flow rate of 2 slpm in the IMR with a volume of about  $45 \text{ cm}^3 (V_{IMR})$ . Under the optimized conditions of the IMR, the pressure ( $P_{actual}$ ) was 70 mbar and the

temperature ( $T_{actual}$ ) was 45°C. The gas flow rate ( $Q_{IMR}$ ) and the residence time can be calculated Eq. S2 and Eq. S3, respectively:

$$Q_{IMR} = \frac{P_0 Q_0}{T_0} \times \frac{T_{actual}}{P_{actual}} \quad (\text{Eq. S2})$$

$$t_{IMR} = \frac{V_{IMR}}{Q_{IMR}} \quad (\text{Eq. S3})$$

60 where  $P_0$  and  $T_0$  are the normal pressure and temperature, and  $Q_0$  is the flow rate of sample gas and reagent ions. Table S3 presents the theoretical sensitivity of the Vocus AIM, which was estimated about 112 ncps/pptv. Our calibration results (Figure S1) indicate that the molecular-ion reaction efficiency in Vocus AIM, calculated via Eq. S4, reached a maximum of approximately 30% for 4-nitrophenol ( $C_6H_5NO_3$ ).

$$reaction\ efficiency = \frac{S_{calibration}}{S_{max}} \quad (\text{Eq. S4})$$

### S1.3 Calibration and Quantification

65 A total of 30 standards were calibrated using permeation tubes and liquid-solution-based techniques for Vocus AIM. These standards can be classified into 5 categories, namely acids (mono-, di- acids), phenols/alcohols (mono-, di- and poly-phenols/alcohols), carbonyl-acids, hydroxyl-acids and nitrophenols. As the Figure S1, the instrumental sensitivities varied between chemicals, with the orders of magnitude ranging from  $10^{-1}$  to  $10^2$  ncps/pptv. For other uncalibrated compounds, an empirical approach based on half of the iodide adducts dissociate ( $dV_{50}$ ), was developed for I-CIMS to extrapolate the  
70 instrumental sensitivities according to our previous studies (He et al., 2024; He et al., 2023).

The sensitivities of 28 authentic standards and corresponding  $dV_{50}$  obtained in our I-CIMS system are plotted in Figure S2. As noted in previous studies, deviations between the observed sensitivities and the values predicted by the log-linear trend may primarily result from the limitations of  $dV_{50}$  in accurately reflecting the effective formation rates of ion-molecule clusters (Lopez-Hilfiker et al., 2016). He et al. proposed a method to estimated sensitivities by considering the ion-molecule  
75 cluster formation in the IMR region as a function of  $dV_{50}$ , mass-dependent transmission efficiency ( $TR$ ), and collision-induced decomposition fraction ( $f$ ) prior to detection (He et al., 2024), as expressed in Eq. S5.

$$S_i = \int_0^t k_f (dV_{50}^i) [I^-] dt \times TR_i \left(\frac{m}{Z}\right) \times f_i \quad (\text{Eq. S5})$$

The effective formation rate of ion-molecule reactions is generally influenced by the chemical functionality and steric configuration of the target molecule (Lee et al., 2014). In this study, calibrating species were classified into groups based on their  $dV_{50}$  values, with each group spanning 1 V (Figure S2). It was assumed that within each category, the formation rate of  
80 ion-molecule clusters remained relatively consistent. As depicted in Figure S2, compounds with  $dV_{50}$  below 3 V were categorized as the first group, most of which contained a single polar functional group like monoacids. The second group, with  $dV_{50}$  values between 3 and 4 V, primarily included compounds with two or more identical hydroxyl or carboxylic groups, such

as diacids and di-/poly-alcohols or phenols. Compounds with  $dV_{50}$  values exceeding 4 V were grouped into the third category, which included most nitro-phenols/alcohols and certain hydroxy-acids. These compounds exhibited enhanced hydrogen-bonding capabilities, increasing their interaction efficiency with I<sup>-</sup>. Linear regression analyses were performed for each  $dV_{50}$  subgroup to correlate the observed sensitivities of standards with the product of the square root of  $m/z$  and fragmentation ratio ( $\sqrt{m/z} \times f$ ), where  $f$  was derived from the fragmentation patterns of the calibrating standards or collision cross-sections from previous research (Zhang et al., 2016; He et al., 2024). The sensitivities calculated via linear fitting showed strong agreement with the measured values for authentic standards, with uncertainties mostly below 40%. For uncalibrated species, the estimated sensitivities using the segmented fitting approach in I<sup>-</sup>-CIMS had uncertainties ranging from approximately 15% to 35%, as listed in Table S10, S11.

#### S1.4 Estimations of Binding Energy

We used the ORCA version 5.0.4 to calculate the binding energies of iodide adducts of BPRs and standards, including formic acid (CH<sub>2</sub>O<sub>2</sub>), 2,4-dihydroxytoluene (C<sub>7</sub>H<sub>8</sub>O<sub>2</sub>), 4-nitrophenol (C<sub>6</sub>H<sub>5</sub>NO<sub>3</sub>), 2-methyl-6-nitrophenol (C<sub>7</sub>H<sub>7</sub>NO<sub>3</sub>) and pinonic acid (C<sub>10</sub>H<sub>16</sub>O<sub>3</sub>). Geometry optimizations and frequency analyses were performed at the B3LYP/ma-def2-TZVP(-f) level with Grimme's D3 dispersion correction, using VeryTightOpt convergence criteria, a maximum of 1000 SCF iterations (VeryTightSCF), DefGrid3 integration grids, and AutoAux-generated auxiliary basis sets for RI acceleration. Single-point energies were computed on the optimized geometries at the DLPNO-CCSD(T)/aug-cc-pVQZ level with TightPNO truncation, VeryTightSCF convergence settings, and the aug-cc-pVQZ/C auxiliary basis sets (with the corresponding ECPs) for RI-JK and RI-MP2 integrals.

## Section S2. Other Relevant Instrumentations

### S2.1 Proton Transfer Reaction Time-of-Flight Mass Spectrometry (PTR-MS)

Aromatic precursors and some gas-phase products were measured using a Tofwerk Vocus proton transfer reaction (PTR) time-of-flight mass spectrometer with a mass resolution of ~10,000. PTR-MS was operated at the pressure of 2.1 mbar in drift tube, applying a voltage of 630 V to achieve an E/N ratio (electric field strength to gas number density) of 120Td, so as to strike a balance between the formation of hydronium water clusters and the fragmentation of product ions. The drift tube was maintained at 100°C, to largely prevent vapor deposition to the wall.

In this study, comprehensive calibrations were performed using a total of 43 representative standards, encompassing volatile organic compounds (VOCs) and intermediate/semi-volatile organic compounds (I/SVOCs) with different functional groups. These standards included hydrocarbons, aldehydes, ketones, alcohols/phenols, carboxylic acids, and furans. Calibrations were performed at 5–6 different concentration levels (from 0.2 to several ppbv), and the sensitivities were determined by the fitting

slopes between instrument signals and the corresponding concentrations, yielding fit values with  $R^2$  ranging from 0.9990 to 0.9999.

For uncalibrated compounds without authentic standards, theoretical sensitivities can be estimated based on the transmission efficiency and proton-transfer reaction rate, as described in our earlier studies (He et al., 2024; He et al., 2023). The response factor of a compound can be expressed by the following Eq. S6.

$$S_{[R]} = \frac{N \times k \times t_R}{10^9} \times \frac{TR_{RH^+}}{TR_{H_3O^+}} \times f \times 10^6 \quad (\text{Eq. S6})$$

[ $R$ ] is the response factor of compound  $R$  in Vocus PTR, which was defined as the ion signal of target compound at a volume mixing ratio of ppbv.  $N$  is the number of air molecules in the drift tube, expressed in unit of molecule/cm<sup>3</sup>,  $k$  is the rate constant of proton-transfer reaction,  $t_R$  refers to the reaction time in the drift tube, and  $f$  means the fragmentation fraction.  $TR_{RH^+}$  and  $TR_{H_3O^+}$  are the ion transmission efficiencies for  $RH^+$  and  $H_3O^+$ , respectively. The values of  $N$  and  $t_R$  can be calculated by working parameters of drift tube.

Ion transmission efficiency in TOF-MS is known to be proportional to the square root of the mass-to-charge ratio ( $m/z$ ) (Yuan et al., 2017). In this study, we used an empirical expression relating ion transmission efficiency to  $m/z$ , as shown in Figure S3, based on existing standards with minimal fragmentation in Vocus PTR. To validate this approach, we compared the calculated response factors with the measured values for different compounds (Figure S4). The results indicated that the calculated response factors were in good agreement with the measured ones, with absolute deviations below 15% (accounting for the fragmentation fraction based on the mass spectra of different compounds). Therefore, we conclude that this method is reliable for estimating the response factors of target oxidation products in the absence of standards.

Uncertainty for the calibrated species was within 10%. For the aromatic oxidation products not calibrated in this study, the uncertainty was anticipated to be higher due to the effects of transmission and fragmentation. The transmission uncertainty for uncalibrated products was quantified by an upper limit of 15% for the relative deviations between the measured and estimated sensitivities of calibrated compounds exhibiting minimal fragmentation (as illustrated in Figure S4). The fragmentation uncertainties for uncalibrated products were determined by comparing the relative deviations in the fragmentation patterns of calibrated compounds with chemically similar structures (He et al., 2024; He et al., 2023). Consequently, the overall uncertainty for uncalibrated products ranged from 15% to 25%, as listed in Table S10, S11.

## S2.2 Traditional Iodide Chemical Ionization Time-of-Flight Mass Spectrometry (Traditional I-CIMS)

Conventional I-CIMS instruments (Aerodyne Research Inc.) were employed for comparative analysis with the Vocus AIM in detecting  $RO_2$  radicals. The iodide reagent ions ( $I^-$ ) were generated by flowing ultra-high purity nitrogen at 2 slpm, doped with methyl iodide, through an X-ray ionization source connected to IMR. A sample flow of 2.3 slpm was introduced into the IMR, where it mixed with the  $I^-$  reagent ion stream to facilitate molecular-ion formation. The instrument demonstrated a mass resolution of  $\sim 5,000$  at 100–500 Th and a total ion count of  $\sim 20,000$  cps.

A total of 54 standards were calibrated using permeation tubes and liquid-solution based techniques. The instrumental sensitivities varied between chemicals, with the orders of magnitude ranging from  $10^{-2}$  to  $10^2$  ncps/ppvtv, which has been described in detail in our previous work (He et al., 2023). Similarly, we estimated the molecular-ion reaction efficiency in traditional I-CIMS via Eq. S4 and it reached a maximum of approximately 10% for 4-nitrophenol ( $C_6H_5NO_3$ ) as Table S3 shows.

### S2.3 Others

$NO_x$ , temperature and relative humidity were monitored by the chemiluminescence analyzer (Model 42i-TL, Thermo Fisher Scientific, USA) and a temperature and humidity sensor. Besides, a laser-induced fluorescence system was used when we calibrated the sensitivity of  $HO_2$  radicals in Vocus AIM. More details are shown in Table S2.

### Section S3. Wall Loss in the Experimental Systems

The wall-induced decay of products from aromatic oxidation was taken into consideration in this study. This process can be described by the first-order reaction kinetic, and the corresponding rate coefficient is expressed as Equation S7 (Zhang et al., 2015; McMurry and Grosjean, 1985).

$$k_{w,i} = \frac{A}{V} \times \frac{\frac{\alpha_{w,i} \bar{v}_i}{4}}{\frac{\pi}{2} \times \frac{\alpha_{w,i} \bar{v}_i}{4\sqrt{D_i K_e}} + 1} \quad (\text{Eq. S7})$$

where the  $k_{w,i}$  is the wall loss rate constant of compound  $i$ .  $A/V$  is the ratio of surface to volume of the tube ( $40 \text{ m}^{-1}$  for the calibration system and  $20 \text{ m}^{-1}$  for the Oxidation Flow Reactor in this study).  $\alpha_{w,i}$  is the mass accommodation coefficient.  $\bar{v}_i$  is the mean thermal speed of molecule  $i$ , related to the temperature and molecular weight, and can be calculated by the Equation S14.  $D_i$  and  $K_e$  refer to the molecular diffusion coefficient and eddy diffusion coefficient, respectively.  $D_i$  in Equation S8 can be calculated by the Equation S9.

$$\bar{v}_i = \sqrt{\frac{8RT}{\pi MW_i}} \quad (\text{Eq. S8})$$

$$D_i = D_{CO_2} \times \frac{MW_{CO_2}}{MW_i} \quad (\text{Eq. S9})$$

where  $R$  represents the ideal gas constant,  $T$  the temperature during the experiments,  $MW_i$  the molecular weight of compound  $i$ ,  $D_{CO_2}$  the molecular diffusion coefficient of  $CO_2$  ( $1.38 \times 10^{-5} \text{ m}^2/\text{s}$ ), and  $MW_{CO_2}$  the molecular weight of  $CO_2$ .

$K_e$  characterized the capacity of turbulent mixing in the reactor. Some estimated values have been given by empirical fittings. For instance, McMurry and Grosjean recommended the  $K_e$  values to be  $0.12 \text{ s}^{-1}$  and  $0.02 \text{ s}^{-1}$  for  $60 \text{ m}^3$  and  $4 \text{ m}^3$  chamber (McMurry and Grosjean, 1985), respectively. Besides, Zhang et al. proposed the smaller  $K_e$  value of  $0.015 \text{ s}^{-1}$  for their  $28 \text{ m}^3$

165 chamber (Zhang et al., 2015), considering the not active mixing. In this study,  $0.0042\text{s}^{-1}$  was adopted due to the nearly equivalent volume in this study compare to the previous research (Huang et al., 2018).

The last unknown parameter  $\alpha_{w,i}$ , representing the fraction of deposited molecules when encountering the wall, is dependent on the molecular property of compound  $i$  in theory. Specifically, vapors with lower volatility are more likely to deposit on the wall (He et al., 2023). Therefore, previous study (Zhang et al., 2015) proposed a set of optimized empirical equations that  
170 related  $\alpha_{w,i}$  to the number of carbon and oxygen atoms contained in the compounds through volatility, as the Equation S10 and S11 shown. That meant  $\alpha_{w,i}$  can be estimated from the chemical composition of the target compounds.

$$\log_{10} \alpha_{w,i} = -0.1919 \times \log_{10} C_i^* - 6.32 \quad (\text{Eq. S10})$$

$$\log_{10} C_i^* = (n_C^0 - n_C^i) b_C - n_O^i b_O - 2 \frac{n_C^i n_O^i}{n_C^i + n_O^i} b_{CO} \quad (\text{Eq. S11})$$

where  $C_i^*$  is the saturation vapor concentration, which can be calculated based on the group-contribution method proposed in the previous study (Nannoolal et al., 2009).  $n_C^0$  is the number of carbon atoms of  $1 \mu\text{g}/\text{m}^3$  alkane,  $b_C$ ,  $b_O$  and  $b_{CO}$  represent the interaction between carbon-carbon atoms, oxygen-oxygen atoms and carbon-oxygen atoms, respectively. Those four  
175 parameters have been determined by Zhang et al (2015), where species were employed to obtain the optimal fitting. The remaining  $n_C^i$  and  $n_O^i$  refer to the number of carbon and oxygen atoms in the target molecule  $i$ , respectively.  $\alpha_{w,i}$  of the aromatic precursors and major tracer products in this study are listed in Table S6.

#### Section S4. Kinetic Reaction Model Analysis of the Calibration System.

M-xylene is selected for the simulation and the kinetic model includes 302 species and 897 reactions from the MCM 3.3.1.  
180 The model is run for 10 seconds in agreement with the residence time of the flow tube reactor with a simulation time resolution of  $10^{-3}$  s. The model is initiated with the measured concentrations of m-xylene (25ppbv), NO (0.5ppbv) and HO<sub>2</sub> radicals ( $7.51 \times 10^{11}$  molecules  $\text{cm}^{-3}$ ) at the exit of the flow tube. The initial OH radical concentration ( $4.5 \times 10^{10}$  molecules  $\text{cm}^{-3}$ ) is tuned in order to match the OH exposure, which was determined from the amount of reacted m-xylene.

Figure S8 shows the temporal evolution of 5 selected species: reacted m-xylene (MXYL<sub>react</sub>), HO<sub>2</sub> radical (HO<sub>2</sub>), BPRs  
185 (MXYBIPERO<sub>2</sub>) as well as 2 products of the m-xylene oxidation with the OH radical (MXYBPEROOH and MXYOBPEROH). MXYBPEROOH (bicyclic hydroperoxide, C<sub>8</sub>H<sub>12</sub>O<sub>5</sub>) is the product from the reaction of BPRs with the HO<sub>2</sub> while MXYOBPEROH (bicyclic carbonyl, C<sub>8</sub>H<sub>10</sub>O<sub>4</sub>) is the main product from the reaction of BPRs + RO<sub>2</sub>. MXYL<sub>react</sub> reaches a plateau after about 0.1 seconds while xylene-BPRs reaches a maximum value around 0.01-0.02 seconds and then rapidly decreases, stabilizes after about 2-4s, consist with the residence time (3-4s) in the calibration reactor.

190 Figure S9 shows the relative contributions of the two main RO<sub>2</sub> radicals, BPRs and MXYLO<sub>2</sub> (C<sub>8</sub>H<sub>9</sub>O<sub>2</sub>), in the calibration experiments. MXYLO is the first-generation RO<sub>2</sub> formed in the benzaldehyde pathway. As shown, BPRs dominate in the initial stage of the reaction, accounting for ~86% of the total RO<sub>2</sub>



## Section S5. Significant Test.

We conducted several repeated experiments of toluene oxidation at toluene levels of 6 ppbv, 12 ppbv and 18 ppbv to evaluate  
195 the reproducibility of our results. As we know, significance analysis typically requires repeated samples. A high level of  
consistency in the branching ratio of bicyclic pathway obtained from the direct-measured method and the products-yield  
method were both observed from these repeated experiment (as shown in Table S13). To further assess the difference between  
the two methods, we conducted statistical *t* tests. The results demonstrated that the branching ratios obtained from the direct-  
measurement method were significantly higher than those from the product-yield method. Comparable results are expected for  
200 the m-xylene system.

## References

- Berndt, T., Hyttinen, N., Herrmann, H., and Hansel, A.: First oxidation products from the reaction of hydroxyl radicals with  
isoprene for pristine environmental conditions, *Commun Chem*, 2, ARTN 21 10.1038/s42004-019-0120-9, 2019.
- 205 He, S. Y., Liu, Y., Song, M. D., Li, X., Lu, S. H., Chen, T. Z., Mu, Y. J., Lou, S. R., Shi, X. D., Qiu, X. H., Zhu, T., and Zhang,  
Y. H.: Insights into the Peroxide-Bicyclic Intermediate Pathway of Aromatic Photooxidation: Experimental Yields and NO<sub>x</sub>-  
Dependency of Ring-Opening and Ring-Retaining Products, *Environ Sci Technol*, 57, 20657-20668, 10.1021/acs.est.3c05304,  
2023.
- He, S. Y., Liu, Y., Song, M. D., Li, X., Lou, S. R., Ye, C. S., Liu, Y. J., Liu, Y., Ye, J. R., Lu, S. H., Zhou, W. X., Qiu, X. H.,  
210 Zhu, T., and Zeng, L. M.: Empirical Approach to Quantifying Sensitivity in Different Chemical Ionization Techniques for  
Organonitrates and Nitroaromatics Constrained by Ion-Molecule Reaction and Transmission Efficiency, *Anal Chem*, 96,  
16882-16890, 10.1021/acs.analchem.4c03751, 2024.
- Huang, Y. L., Zhao, R., Charan, S. M., Kenseth, C. M., Zhang, X., and Seinfeld, J. H.: Unified Theory of Vapor-Wall Mass  
Transport in Teflon-Walled Environmental Chambers, *Environ. Sci. Technol.*, 52, 2134-2142, 10.1021/acs.est.7b05575, 2018.
- 215 Isaacman-VanWertz, G., Massoli, P., O'Brien, R., Lim, C., Franklin, J. P., Moss, J. A., Hunter, J. F., Nowak, J. B., Canagaratna,  
M. R., Misztal, P. K., Arata, C., Roscioli, J. R., Herndon, S. T., Onasch, T. B., Lambe, A. T., Jayne, J. T., Su, L. P., Knopf, D.  
A., Goldstein, A. H., Worsnop, D. R., and Kroll, J. H.: Chemical evolution of atmospheric organic carbon over multiple  
generations of oxidation, *Nat Chem*, 10, 462-468, 10.1038/s41557-018-0002-2, 2018.
- Lee, B. H., Lopez-Hilfiker, F. D., Mohr, C., Kurtén, T., Worsnop, D. R., and Thornton, J. A.: An Iodide-Adduct High-  
220 Resolution Time-of-Flight Chemical-Ionization Mass Spectrometer: Application to Atmospheric Inorganic and Organic  
Compounds, *Environ Sci Technol*, 48, 6309-6317, 10.1021/es500362a, 2014.
- Lopez-Hilfiker, F. D., Iyer, S., Mohr, C., Lee, B. H., D'Ambro, E. L., Kurtén, T., and Thornton, J. A.: Constraining the  
sensitivity of iodide adduct chemical ionization mass spectrometry to multifunctional organic molecules using the collision  
limit and thermodynamic stability of iodide ion adducts, *Atmos Meas Tech*, 9, 1505-1512, 10.5194/amt-9-1505-2016, 2016.
- 225 Martín, P., Cabañas, B., Colmenar, I., Salgado, M. S., Villanueva, F., and Tapia, A.: Reactivity of E-butenedial with the major  
atmospheric oxidants, *Atmos Environ*, 70, 351-360, 10.1016/j.atmosenv.2013.01.041, 2013.
- Mcmurry, P. H. and Grosjean, D.: Gas and Aerosol Wall Losses in Teflon Film Smog Chambers, *Environ Sci Technol*, 19,  
1176-1182, DOI 10.1021/es00142a006, 1985.
- Nannoolal, Y., Rarey, J., and Ramjugernath, D.: Estimation of pure component properties. Part 4: Estimation of the saturated  
230 liquid viscosity of non-electrolyte organic compounds via group contributions and group interactions, *Fluid Phase Equilibr*,  
281, 97-119, 10.1016/j.fluid.2009.02.016, 2009.
- Perry, R. A., Atkinson, R., and Pitts, J. N.: Kinetics and Mechanism of Gas-Phase Reaction of Oh Radicals with  
Methoxybenzene and O-Cresol over Temperature-Range 299-435-K, *J Phys Chem-US*, 81, 1607-1611, DOI  
10.1021/j100532a001, 1977.

- 235 Sharma, S. B., Mudaliar, M., Rao, B. S. M., Mohan, H., and Mittal, J. P.: Radiation chemical oxidation of benzaldehyde, acetophenone, and benzophenone, *J Phys Chem A*, 101, 8402-8408, DOI 10.1021/jp9718717, 1997.
- Wang, S. N., Riva, M., Yan, C., Ehn, M., and Wang, L. M.: Primary Formation of Highly Oxidized Multifunctional Products in the OH-Initiated Oxidation of Isoprene: A Combined Theoretical and Experimental Study, *Environ Sci Technol*, 52, 12255-12264, 10.1021/acs.est.8b02783, 2018.
- 240 Wang, Y. H., Hu, R. Z., Xie, P. H., Chen, H., Wang, F. Y., Liu, X. Y., Liu, J. G., and Liu, W. Q.: Measurement of tropospheric HO<sub>x</sub> radical using fluorescence assay by gas expansion with low interferences, *J Environ Sci*, 99, 40-50, 10.1016/j.jes.2020.06.010, 2021.
- Yuan, B., Koss, A. R., Warneke, C., Coggon, M., Sekimoto, K., and de Gouw, J. A.: Proton-Transfer-Reaction Mass Spectrometry: Applications in Atmospheric Sciences, *Chem Rev*, 117, 13187-13229, 10.1021/acs.chemrev.7b00325, 2017.
- 245 Zhang, X., Schwantes, R. H., McVay, R. C., Lignell, H., Coggon, M. M., Flagan, R. C., and Seinfeld, J. H.: Vapor wall deposition in Teflon chambers, *Atmos Chem Phys*, 15, 4197-4214, 10.5194/acp-15-4197-2015, 2015.
- Zhang, X., Krechmer, J. E., Groessl, M., Xu, W., Graf, S., Cubison, M., Jayne, J. T., Jimenez, J. L., Worsnop, D. R., and Canagaratna, M. R.: A novel framework for molecular characterization of atmospherically relevant organic compounds based on collision cross section and mass-to-charge ratio, *Atmos. Chem. Phys.*, 16, 12945-12959, 10.5194/acp-16-12945-2016, 2016.
- 250 Zhao, Y., Thornton, J. A., and Pye, H. O. T.: Quantitative constraints on autoxidation and dimer formation from direct probing of monoterpene-derived peroxy radical chemistry, *P Natl Acad Sci USA*, 115, 12142-12147, 10.1073/pnas.1812147115, 2018.

**Table S1. Calibration System: experimental conditions of aromatic-RO<sub>2</sub> calibrations.**

Expt NO.	Reactants	Temperature [°C]	Relative Humidity [%]	OH <sub>av</sub> [molecule/cm <sup>3</sup> ]
1	5ppb TOL	25±1	40±5	1.43×10 <sup>10</sup>
2	10ppb TOL	25±1	40±5	1.46×10 <sup>10</sup>
3	15ppb TOL	25±1	40±5	1.23×10 <sup>10</sup>
4	20ppb TOL	25±1	40±5	1.23×10 <sup>10</sup>
5	10ppb m-XYL	25±1	40±5	5.50×10 <sup>9</sup>
6	15ppb m-XYL	25±1	40±5	5.31×10 <sup>9</sup>
7	20ppb m-XYL	25±1	40±5	6.10×10 <sup>9</sup>
8	25ppb m-XYL	25±1	40±5	6.31×10 <sup>9</sup>

\*The calibrations were conducted under essentially fixed low-NO<sub>x</sub> (~ 0.5 ppbv) and high-HO<sub>2</sub> (~10<sup>11</sup> molecular/cm<sup>3</sup>) conditions, by adjusting the precursor concentration to vary the NO/precursor ratio, to determine whether RO<sub>2</sub> radicals can proceed linearly.

**Table S2. Instrumentations in this study.**

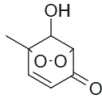
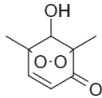
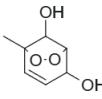
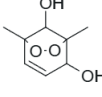
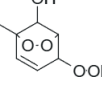
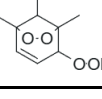
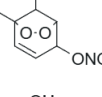
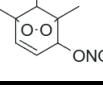
Instrument	Detection limit	Time resolution	Sampling flow rate
Vocus AIM (Tofwerk, Switzerland)	~pptv	1s	~2L/min
Vocus PTR (Tofwerk, Switzerland)	~pptv	1s	~100mL/min
NO <sub>x</sub> analyzer (Model 42i-TL, Thermo Fisher Scientific, USA)	~100pptv	1min	~1L/min
HO <sub>x</sub> -LIF (Wang et al., 2021)*	~0.1pptv	1min	~2L/min

\*: The calibration of Vocus AIM for HO<sub>2</sub> is performed utilizing the LIF (Laser-Induced Fluorescence) instrumentation at Anhui Institute of Optics and Fine Mechanics. The calibration results are listed in Figure S5.

**Table S3. Theoretical sensitivity of Vocus AIM and traditional I-CIMS.**

	Vocus AIM	Traditional I-CIMS(He et al., 2023)
$P_{actual}$	70 mbar	380 mbar
$T_{actual}$	45°C	30°C
$Q_{all}$	2.25 L/min	4 L/min
$V_{IMR}$	~45 cm <sup>3</sup>	~ 47 cm <sup>3</sup>
$[M]_{IMR}$	$1.59 \times 10^{18}$ molecules/cm <sup>3</sup>	$9.08 \times 10^{18}$ molecules/cm <sup>3</sup>
$f$	0.88	0.5
$t_{IMR}$	0.08	0.24
$S_{max}$	112 ncps/pptv	1090 ncps/pptv
Sen. for C <sub>6</sub> H <sub>5</sub> NO <sub>3</sub>	37 ncps/pptv	66 cps/pptv

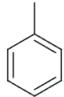
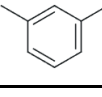
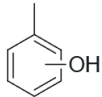
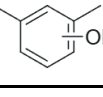
**Table S4. Information of aromatics and their tracer products detected by Vocus AIM (I-CIMS).**

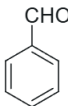
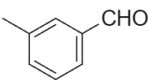
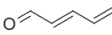
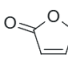
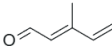
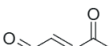
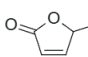
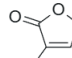
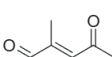
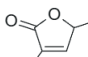
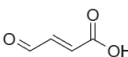
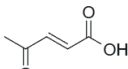
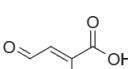
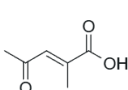
Class	Formula	Ion mass [amu]	Compound	Structure	Sensitivity [ncps/pptv]
1 <sup>e</sup>	C <sub>7</sub> H <sub>8</sub> O <sub>4</sub>	157.05	Bicyclic carbonyl		7.8
	C <sub>8</sub> H <sub>10</sub> O <sub>4</sub>	171.07	Bicyclic carbonyl		8.7
2 <sup>e</sup>	C <sub>7</sub> H <sub>10</sub> O <sub>4</sub>	159.06	Bicyclic alcohol		9.8
	C <sub>8</sub> H <sub>12</sub> O <sub>4</sub>	173.08	Bicyclic alcohol		10.7
3 <sup>e</sup>	C <sub>7</sub> H <sub>10</sub> O <sub>5</sub>	175.05	Bicyclic hydroperoxide		11.4
	C <sub>8</sub> H <sub>12</sub> O <sub>5</sub>	189.07	Bicyclic hydroperoxide		14.3
4 <sup>e</sup>	C <sub>7</sub> H <sub>9</sub> NO <sub>6</sub>	186.04	Bicyclic nitrate		18
	C <sub>8</sub> H <sub>11</sub> NO <sub>6</sub>	218.07	Bicyclic nitrate		20.1

<sup>e</sup> Ring-retaining products from peroxide-bicyclic intermediate pathway.

\* Sensitivity was obtained from calibration.

**Table S5. Information of aromatics and their tracer products detected by Vocus PTR.**

Class	Formula	Ion mass [amu]	Compound	Structure	Sensitivity [cps/ppbv]
1 <sup>a</sup>	C <sub>7</sub> H <sub>8</sub>	93.07	Toluene		14766
	C <sub>8</sub> H <sub>10</sub>	107.09	m-Xylene		17280
2 <sup>b</sup>	C <sub>7</sub> H <sub>8</sub> O	109.06	Cresol		17797
	C <sub>8</sub> H <sub>10</sub> O	123.08	2,6-Dimethylphenol		18103

3 <sup>c</sup>	C <sub>7</sub> H <sub>6</sub> O	107/05	Benzaldehyde		11891
	C <sub>8</sub> H <sub>8</sub> O	121.06	3-Methylbenzaldehyde		11443
4 <sup>d</sup>	C <sub>4</sub> H <sub>4</sub> O <sub>2</sub>	85/03	Butene dial		17604
	C <sub>4</sub> H <sub>4</sub> O <sub>2</sub>	85.03	2(5H)-Furanone		9929
	C <sub>5</sub> H <sub>6</sub> O <sub>2</sub>	99.04	2-Methylbutenedial		18169
	C <sub>5</sub> H <sub>6</sub> O <sub>2</sub>	99.04	4-Oxo-2-pentenal		18169
	C <sub>5</sub> H <sub>6</sub> O <sub>2</sub>	99.04	5-Methyl-2(5H)-furanone		10223
	C <sub>5</sub> H <sub>6</sub> O <sub>2</sub>	99.04	3-Methyl-2(5H)-furanone		10223
	C <sub>6</sub> H <sub>8</sub> O <sub>2</sub>	113.06	Methyl-4-oxo-2-pentenal		18489
	C <sub>6</sub> H <sub>8</sub> O <sub>2</sub>	113.06	3,5-Dimethyl-2(5H)-furanone		10734
	C <sub>4</sub> H <sub>4</sub> O <sub>3</sub>	101.02	Male aldehydic acid		10741
	C <sub>5</sub> H <sub>6</sub> O <sub>3</sub>	115.04	4-Oxo-pent-2-enoic acid		11826
	C <sub>5</sub> H <sub>6</sub> O <sub>3</sub>	115.04	2-Methyl-4-oxobut-2-enoic acid		11826
C <sub>6</sub> H <sub>8</sub> O <sub>3</sub>	129.05	Acetyl methacrylic acid		12101	

a Aromatic precursors.

b Ring-retaining products from phenolic pathway.

c Ring-retaining products from benzaldehyde pathway.

d Ring-opening products from peroxide-bicyclic intermediate pathway.

\* Sensitivity was obtained from calibration.

**Table S6. Wall accommodation coefficients and wall loss rates of aromatic precursors and major tracer products.**

NO.	Formula	Wall accommodation coefficient ( $\alpha_w$ )	Wall loss rate ( $k_w, s^{-1}$ )
1	C <sub>7</sub> H <sub>8</sub>	$1.14 \times 10^{-8}$	$9.39 \times 10^{-7}$
2	C <sub>8</sub> H <sub>10</sub>	$1.37 \times 10^{-8}$	$1.05 \times 10^{-6}$
3	C <sub>7</sub> H <sub>8</sub> O	$2.23 \times 10^{-8}$	$1.70 \times 10^{-6}$
4	C <sub>7</sub> H <sub>6</sub> O	$2.23 \times 10^{-8}$	$1.71 \times 10^{-6}$
5	C <sub>8</sub> H <sub>10</sub> O	$2.65 \times 10^{-8}$	$1.90 \times 10^{-6}$
6	C <sub>8</sub> H <sub>8</sub> O	$2.65 \times 10^{-8}$	$1.91 \times 10^{-6}$
8	C <sub>4</sub> H <sub>4</sub> O <sub>2</sub>	$3.03 \times 10^{-8}$	$2.61 \times 10^{-6}$
9	C <sub>5</sub> H <sub>6</sub> O <sub>2</sub>	$3.48 \times 10^{-8}$	$2.78 \times 10^{-6}$
10	C <sub>6</sub> H <sub>8</sub> O <sub>2</sub>	$4.03 \times 10^{-8}$	$3.01 \times 10^{-6}$
11	C <sub>4</sub> H <sub>4</sub> O <sub>3</sub>	$7.26 \times 10^{-8}$	$5.73 \times 10^{-6}$
12	C <sub>5</sub> H <sub>6</sub> O <sub>3</sub>	$8.10 \times 10^{-8}$	$5.99 \times 10^{-6}$
13	C <sub>6</sub> H <sub>8</sub> O <sub>3</sub>	$9.19 \times 10^{-8}$	$6.41 \times 10^{-6}$
14	C <sub>7</sub> H <sub>8</sub> O <sub>4</sub>	$2.45 \times 10^{-7}$	$1.55 \times 10^{-5}$
15	C <sub>8</sub> H <sub>10</sub> O <sub>4</sub>	$2.42 \times 10^{-7}$	$1.17 \times 10^{-5}$
16	C <sub>7</sub> H <sub>10</sub> O <sub>4</sub>	$2.45 \times 10^{-7}$	$1.54 \times 10^{-5}$
17	C <sub>8</sub> H <sub>12</sub> O <sub>4</sub>	$2.42 \times 10^{-7}$	$1.17 \times 10^{-5}$
18	C <sub>7</sub> H <sub>10</sub> O <sub>5</sub>	$2.45 \times 10^{-7}$	$1.46 \times 10^{-5}$
19	C <sub>8</sub> H <sub>12</sub> O <sub>5</sub>	$2.42 \times 10^{-7}$	$1.12 \times 10^{-5}$
20	C <sub>7</sub> H <sub>9</sub> O <sub>5</sub>	$2.53 \times 10^{-5}$	$1.47 \times 10^{-3}$
21	C <sub>8</sub> H <sub>11</sub> O <sub>5</sub>	$2.48 \times 10^{-5}$	$1.46 \times 10^{-3}$

Table S7. Calibration System: branching ratios of different reaction pathways in calibrations.

Aromatic precursor	Conditions	Branching ratios of different reaction pathways (%)									
		Benzaldehyde pathway	Phenolic pathway	Peroxide-bicyclic intermediate pathway							
	NO/TOL	C <sub>7</sub> H <sub>6</sub> O	C <sub>7</sub> H <sub>8</sub> O	C <sub>4</sub> H <sub>4</sub> O <sub>2</sub>	C <sub>5</sub> H <sub>6</sub> O <sub>2</sub>	C <sub>4</sub> H <sub>4</sub> O <sub>3</sub>	C <sub>5</sub> H <sub>6</sub> O <sub>3</sub>	C <sub>7</sub> H <sub>8</sub> O <sub>4</sub>	C <sub>7</sub> H <sub>10</sub> O <sub>4</sub>	C <sub>7</sub> H <sub>10</sub> O <sub>5</sub>	SUM
TOL	0.08	5.3	18.4	4.7	9.7	3.9	2.1	23	3.2	21.9	68.5
	0.04	5.4	18.4	4.6	9.1	4	1.7	23.1	3.6	21.8	67.9
	0.03	5.4	18.8	4.9	8.6	4	1.7	22.4	3.5	21.8	66.9
	0.02	5.4	18.9	4.6	8.2	3.8	1.9	22.9	3.5	22	66.9
	NO/m-XYL	C <sub>8</sub> H <sub>8</sub> O	C <sub>8</sub> H <sub>10</sub> O	C <sub>5</sub> H <sub>6</sub> O <sub>2</sub>	C <sub>6</sub> H <sub>8</sub> O <sub>2</sub>	C <sub>5</sub> H <sub>6</sub> O <sub>3</sub>	C <sub>6</sub> H <sub>8</sub> O <sub>3</sub>	C <sub>8</sub> H <sub>10</sub> O <sub>4</sub>	C <sub>8</sub> H <sub>12</sub> O <sub>4</sub>	C <sub>8</sub> H <sub>12</sub> O <sub>5</sub>	SUM
m-XYL	0.1	2.8	8.8	23.5	6.0	3.2	1.5	24.7	5.7	21.5	86.1
	0.08	2.8	8.8	23.3	5.9	3.2	2.2	24.4	5.9	21.0	85.9
	0.04	3.1	8.9	23.0	6.4	3.4	3.0	23.0	5.6	21.2	85.6
	0.02	3.1	8.8	23.6	6.3	3.4	2.7	23.0	5.8	21.1	85.9

Table S8. Oxidation Flow Reactor: branching ratios of different reaction pathways in toluene oxidation.

Aromatic precursor	Conditions	Branching ratios of different reaction pathways (%)									
		Benzaldehyde pathway	Phenolic pathway	Peroxide-bicyclic intermediate pathway							
				Product-yield method					Direct-measured method		
	NO/TOL	C <sub>7</sub> H <sub>6</sub> O	C <sub>7</sub> H <sub>8</sub> O	C <sub>4</sub> H <sub>4</sub> O <sub>2</sub>	C <sub>5</sub> H <sub>6</sub> O <sub>2</sub>	C <sub>4</sub> H <sub>4</sub> O <sub>3</sub>	C <sub>5</sub> H <sub>6</sub> O <sub>3</sub>	C <sub>7</sub> H <sub>8</sub> O <sub>4</sub>	C <sub>7</sub> H <sub>10</sub> O <sub>4</sub>	C <sub>7</sub> H <sub>10</sub> O <sub>5</sub>	C <sub>7</sub> H <sub>9</sub> O <sub>5</sub>
TOL	0.03	11.7	20.9	6.1	26.2	2.2	2.3	4.4	0.6	3.2	54.0
	0.04	11.3	21.2	6.1	26.6	2.2	2.4	4.6	0.8	3.4	54.9
	0.06	11.3	22.6	6.5	28.6	2.2	2.7	5.0	0.6	3.7	57.5
	0.1	10.3	22.2	6.5	29.4	2.0	2.8	5.3	0.8	4.0	57.9
	0.2	9.4	22.3	7.5	30.8	2.0	3.4	6.4	1.1	4.8	63.3

Table S9. Oxidation Flow Reactor: branching ratios of different reaction pathways in m-xylene oxidation.

Aromatic precursor	Conditions	Branching ratios of different reaction pathways (%)									
		Benzaldehyde pathway	Phenolic pathway	Peroxide-bicyclic intermediate pathway							
				Product-yield method					Direct-measured method		
	NO/m-XYL	C <sub>8</sub> H <sub>8</sub> O	C <sub>8</sub> H <sub>10</sub> O	C <sub>5</sub> H <sub>6</sub> O <sub>2</sub>	C <sub>6</sub> H <sub>8</sub> O <sub>2</sub>	C <sub>5</sub> H <sub>6</sub> O <sub>3</sub>	C <sub>6</sub> H <sub>8</sub> O <sub>3</sub>	C <sub>8</sub> H <sub>10</sub> O <sub>4</sub>	C <sub>8</sub> H <sub>12</sub> O <sub>4</sub>	C <sub>8</sub> H <sub>12</sub> O <sub>5</sub>	C <sub>8</sub> H <sub>11</sub> O <sub>5</sub>
m-XYL	0.07	5.5	5.8	28.7	14.8	1.4	1.0	5.1	2.3	6.0	67.7
	0.09	5.3	6.0	29.9	15.8	1.4	0.7	5.5	2.3	5.9	68.7
	0.12	4.8	6.0	30.0	16.6	1.3	0.9	5.4	2.2	5.9	68.5
	0.19	4.3	6.1	30.2	18.6	1.4	0.9	5.4	2.2	5.8	69.4
	0.4	3.6	6.0	30.4	24.2	1.4	0.8	5.9	2.2	5.8	73.4



**Table S10. Measurement uncertainty contributions in tol-BPRs calibration.**

NO	Formula	Compound	Measurement uncertainty	Loss uncertainty		Total uncertainty
			Sensitivity	Wall loss (Zhang et al., 2015)	OH reaction	
1	C <sub>7</sub> H <sub>8</sub> O	Cresol	9.50%	15%	10.0% <sup>a</sup>	20.38%
2	C <sub>7</sub> H <sub>6</sub> O	Benzaldehyde	7.60%	15%	5.8% <sup>b</sup>	17.79%
3	C <sub>7</sub> H <sub>8</sub> O <sub>4</sub>	Bicyclic carbonyl	22%	15%	10%	28.44%
4	C <sub>7</sub> H <sub>10</sub> O <sub>4</sub>	Bicyclic alcohol	22%	15%	10%	28.44%
5	C <sub>7</sub> H <sub>10</sub> O <sub>5</sub>	Bicyclic hydroperoxide	22%	15%	10%	28.44%
6	C <sub>4</sub> H <sub>4</sub> O <sub>2</sub>	Butene dial	20%	15%	4.9% <sup>c</sup>	25.48%
7	C <sub>4</sub> H <sub>4</sub> O <sub>2</sub>	2(5H)-Furanone	18%	15%	10%	25.48%
8	C <sub>5</sub> H <sub>6</sub> O <sub>2</sub>	2-Methylbutenedial	18%	15%	10%	25.48%
9	C <sub>5</sub> H <sub>6</sub> O <sub>2</sub>	4-Oxo-2-pentenal	18%	15%	1.9% <sup>e</sup>	23.51%
10	C <sub>5</sub> H <sub>6</sub> O <sub>2</sub>	5-Methyl-2(5H)-furanone	16%	15%	10%	24.10%
11	C <sub>5</sub> H <sub>6</sub> O <sub>2</sub>	3-Methyl-2(5H)-furanone	7%	15%	10%	19.34%
12	C <sub>4</sub> H <sub>4</sub> O <sub>3</sub>	Malealdehydic acid	21%	15%	10%	27.68%
13	C <sub>5</sub> H <sub>6</sub> O <sub>3</sub>	4-Oxo-pent-2-enoic acid	21%	15%	10%	27.68%
14	C <sub>5</sub> H <sub>6</sub> O <sub>3</sub>	2-Methyl-4-oxobut-2-enoic acid	21%	15%	10%	27.68%
15	The branching ratio of RO <sub>2</sub> pathway, $\alpha$		-	-	-	24.87%

<sup>a</sup> Refers to (Perry et al., 1977)

<sup>b</sup> Refers to (Sharma et al., 1997)

<sup>c</sup> Refers to (Martín et al., 2013)

**Table S11. Measurement uncertainty contributions in m-xyl-BPRs calibration.**

NO	Formula	Compound	Measurement uncertainty	Loss uncertainty		Total uncertainty
			Sensitivity	Wall loss (Zhang et al., 2015)	OH reaction	
1	C <sub>8</sub> H <sub>10</sub> O	2,6-Dimethylphenol	10%	15%	5.1% <sup>a</sup>	18.74%
2	C <sub>8</sub> H <sub>8</sub> O	3-Mehtylbenzaldehyde	10%	15%	5.8% <sup>b</sup>	18.94%
3	C <sub>8</sub> H <sub>10</sub> O <sub>4</sub>	Bicyclic carbonyl	20%	15%	10%	26.93%
4	C <sub>8</sub> H <sub>12</sub> O <sub>4</sub>	Bicyclic alcohol	20%	15%	10%	26.93%
5	C <sub>8</sub> H <sub>12</sub> O <sub>5</sub>	Bicyclic hydroperoxide	20%	15%	10%	26.93%
6	C <sub>5</sub> H <sub>6</sub> O <sub>2</sub>	2-Methylbutenedial	18%	15%	10%	25.48%
7	C <sub>5</sub> H <sub>6</sub> O <sub>2</sub>	4-Oxo-2-pental	18%	15%	1.9% <sup>c</sup>	23.51%
8	C <sub>5</sub> H <sub>6</sub> O <sub>2</sub>	5-Methyl-2(5H)-furanone	16%	15%	10%	24.10%
9	C <sub>5</sub> H <sub>6</sub> O <sub>2</sub>	3-Methyl-2(5H)-furanone	7%	15%	10%	19.34%
10	C <sub>6</sub> H <sub>8</sub> O <sub>2</sub>	Methyl-4-oxo-2-pental	18%	15%	10%	25.48%
11	C <sub>6</sub> H <sub>8</sub> O <sub>2</sub>	3,5-Dimethy-2(5H)-furanone	16%	15%	10%	24.10%
12	C <sub>5</sub> H <sub>6</sub> O <sub>3</sub>	4-Oxo-pent-2-enoic acid	21%	15%	10%	27.68%
13	C <sub>5</sub> H <sub>6</sub> O <sub>3</sub>	2-Methyl-4-oxobut-2-enoic acid	21%	15%	10%	27.68%
14	C <sub>6</sub> H <sub>8</sub> O <sub>3</sub>	Acetyl methacrylic acid	21%	15%	10%	27.68%
15	The branching ratio of RO <sub>2</sub> pathway, $\alpha$		-	-	-	24.42%

<sup>a</sup> Refers to (Perry et al., 1977)

<sup>b</sup> Refers to (Sharma et al., 1997)

<sup>c</sup> Refers to (Martín et al., 2013)

**Table S12. Calibration results for Vocus AIM in this study.**

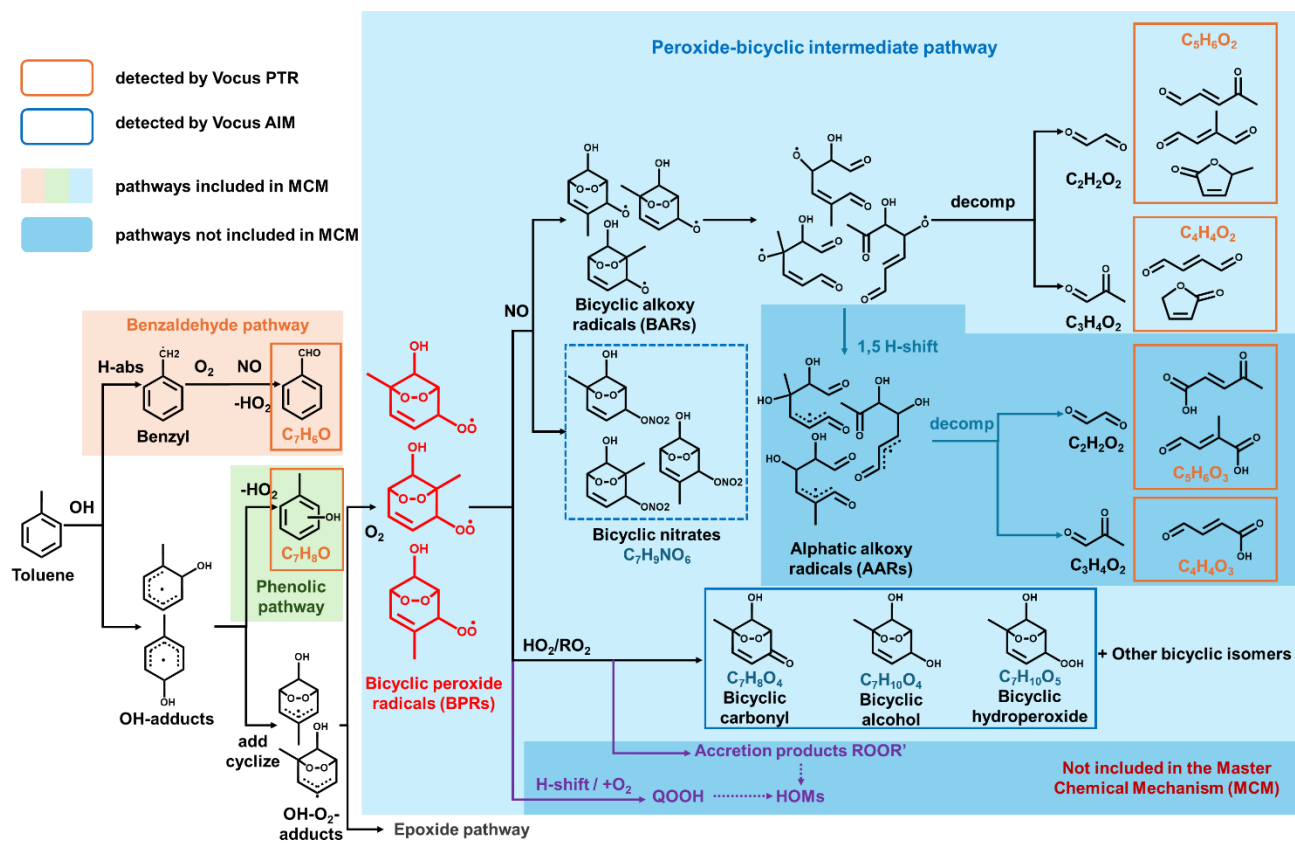
Species	Formula	Sensitivity (ncps/ppt)	Category
Glycerol	C <sub>3</sub> H <sub>8</sub> O <sub>3</sub>	51.81	di/poly alcohols/phenols
Pentanedioic acid	C <sub>5</sub> H <sub>8</sub> O <sub>4</sub>	2.65	diacids
Azelaic acid	C <sub>9</sub> H <sub>16</sub> O <sub>4</sub>	3.18	diacids
D(+)-Camphoric acid	C <sub>10</sub> H <sub>14</sub> O <sub>4</sub>	3.64	diacids
Heptanedioic acid	C <sub>7</sub> H <sub>12</sub> O <sub>4</sub>	4.03	diacids
Formic acid	CH <sub>2</sub> O <sub>2</sub>	3.13	diacids
Hexanedioic acid	C <sub>6</sub> H <sub>10</sub> O <sub>4</sub>	4.54	diacids
Octanedioic acid	C <sub>8</sub> H <sub>14</sub> O <sub>4</sub>	16.51	diacids
Decanedioic acid	C <sub>10</sub> H <sub>18</sub> O <sub>4</sub>	17.51	diacids
O-Benzendicarboxylic Acid	C <sub>8</sub> H <sub>6</sub> O <sub>4</sub>	0.40	hydroxy-acids
Citric Acid	C <sub>6</sub> H <sub>10</sub> O <sub>4</sub>	3.18	hydroxy-acids
Glycolic acid	C <sub>2</sub> H <sub>4</sub> O <sub>3</sub>	3.25	hydroxy-acids
2-Deoxy-D-ribose	C <sub>5</sub> H <sub>10</sub> O <sub>4</sub>	5.44	hydroxy-acids
2-Hydroxy-2-methylbutyric acid	C <sub>5</sub> H <sub>10</sub> O <sub>3</sub>	5.69	hydroxy-acids
Salicylic acid	C <sub>7</sub> H <sub>6</sub> O <sub>3</sub>	14.37	hydroxy-acids
Leucic acid	C <sub>6</sub> H <sub>12</sub> O <sub>3</sub>	16.51	hydroxy-acids
Lactic acid	C <sub>3</sub> H <sub>6</sub> O <sub>3</sub>	19.90	hydroxy-acids
Pentadecanoic acid	C <sub>15</sub> H <sub>30</sub> O <sub>2</sub>	0.51	mono-acids
Heptadecanoic acid	C <sub>17</sub> H <sub>34</sub> O <sub>2</sub>	0.53	mono-acids
Tridecanoic acid	C <sub>13</sub> H <sub>26</sub> O <sub>2</sub>	0.65	mono-acids
Undecanoic acid	C <sub>11</sub> H <sub>22</sub> O <sub>2</sub>	0.67	mono-acids
2-Nitrophenol	C <sub>6</sub> H <sub>5</sub> NO <sub>3</sub>	0.06	nitro-phenols/alcohols
Isosorbide mononitrate	C <sub>6</sub> H <sub>9</sub> NO <sub>6</sub>	0.42	nitro-phenols/alcohols
2-Nitroethanol	C <sub>2</sub> H <sub>5</sub> NO <sub>3</sub>	6.13	nitro-phenols/alcohols
5-Methyl-2-nitrophenol	C <sub>7</sub> H <sub>7</sub> NO <sub>3</sub>	17.30	nitro-phenols/alcohols
4-Nitrophenol	C <sub>6</sub> H <sub>5</sub> NO <sub>3</sub>	38.00	nitro-phenols/alcohols
2-methyl-4-nitrosophenol	C <sub>7</sub> H <sub>7</sub> NO <sub>3</sub>	48.03	nitro-phenols/alcohols
2,6-Dimethyl-4-nitrophenol	C <sub>8</sub> H <sub>9</sub> NO <sub>3</sub>	60.29	nitro-phenols/alcohols
Pinonic acid	C <sub>10</sub> H <sub>16</sub> O <sub>3</sub>	1.00	oxo-monoacids
Acetylpropionic acid	C <sub>5</sub> H <sub>8</sub> O <sub>3</sub>	7.10	oxo-monoacids

**Table S13. Significance test for the branching ratio of bicyclic pathway by the direct method and the product-yield method at different precursor concentration.**

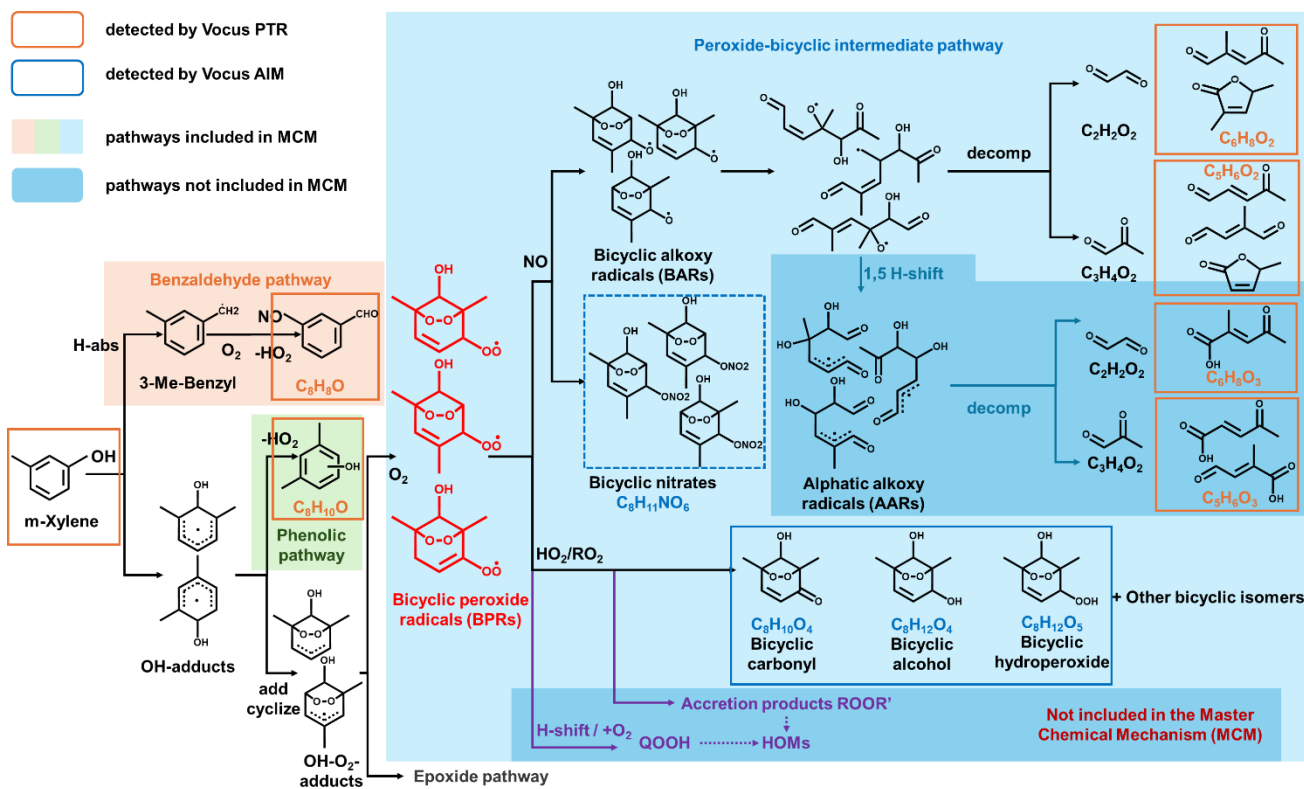
Toluene (ppbv)	Method	Branching ratio (%)				Shapiro-Wilk test	<i>t</i> test
		Exp.1	Exp.2	Exp.3	Mean		
6	D <sup>a</sup>	63.3	60.4	60.6	61.4±1.3	p = 0.129 > 0.05	$H_0: \mu_D \leq \mu_Y$
	Y <sup>b</sup>	55.9	52.9	55.5	54.8±1.3	p = 0.218 > 0.05	$H_A: \mu_D > \mu_Y$ p = 0.0036 < 0.05
12	D	58.0	57.2	56.1	57.1±0.8	p = 0.749 > 0.05	$H_0: \mu_D \leq \mu_Y$
	Y	50.8	49.2	49.4	49.8±0.7	p = 0.253 > 0.05	$H_A: \mu_D > \mu_Y$ p = 0.0003 < 0.05
18	D	57.5	56.2	56.5	56.7±0.6	p = 0.562 > 0.05	$H_0: \mu_D \leq \mu_Y$
	Y	49.3	49.4	48.7	49.1±0.3	p = 0.209 > 0.05	$H_A: \mu_D > \mu_Y$ p = 0.002 < 0.05

10

15



Scheme S1. Chemical mechanism for toluene-OH oxidation.



Scheme S2. Chemical mechanism for m-xylene-OH oxidation.

25

30

35

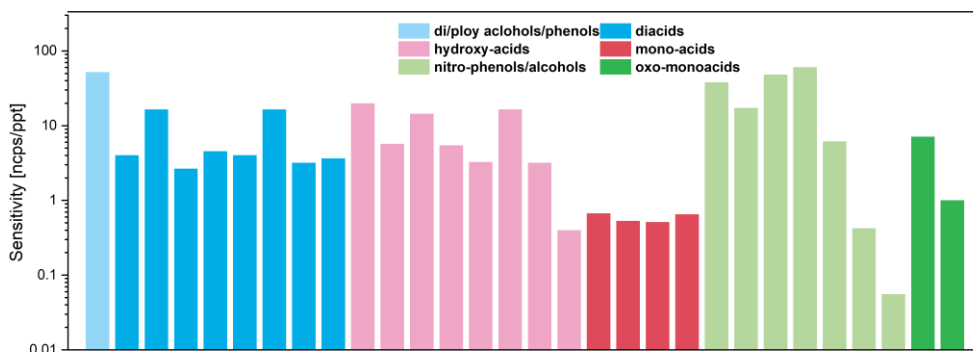
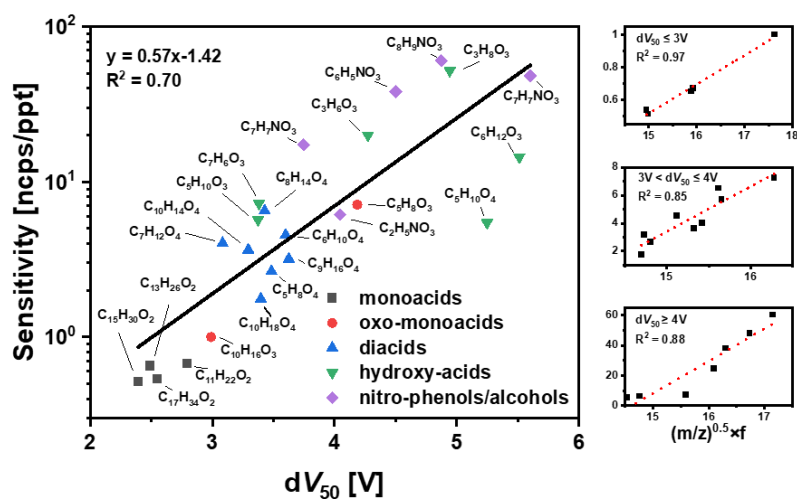
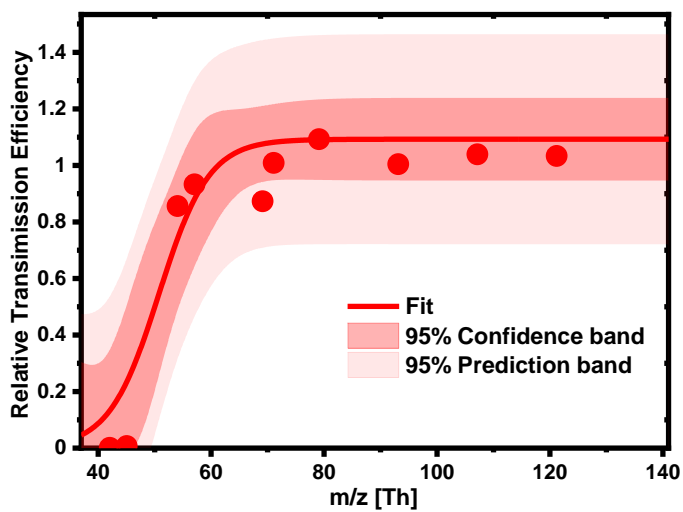


Figure S1. Calibration results for Vocus AIM in this study.



45

Figure S2 Relationship between the sensitivities and the corresponding  $dV_{50}$  values of standards in the AIM-CIMS (left).  $dV_{50}$ -based segmented linear fitting of the sensitivity and the product of the square root of  $m/z$  and fragmentation ratio (right).



50

Figure S3 Relationship between relative transmission efficiencies of ions and their mass-to-charge ratios ( $m/z$ ).

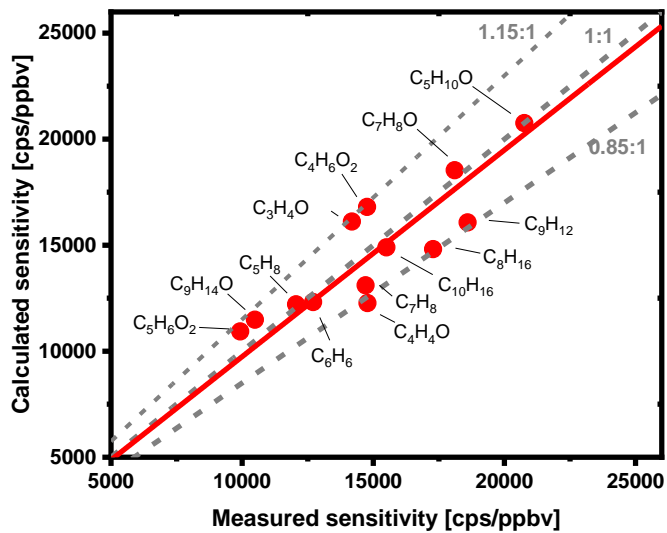
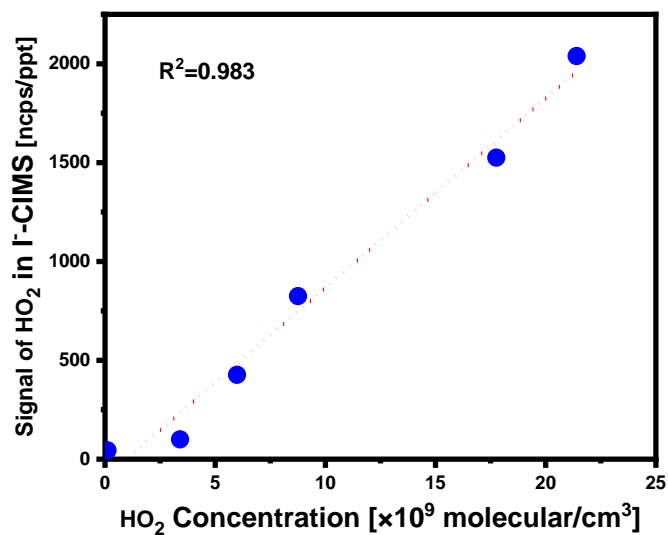


Figure S4 Comparison of calculated and measured sensitivities for different classes of compounds.

55





**Figure S5 Calibration of the sensitivity of HO<sub>2</sub> radical by Vocus AIM**

\*: The concentration of HO<sub>2</sub> radicals was quantitatively determined utilizing LIF. Details about this instrument can be found in the previous reference(Wang et al., 2021).

60

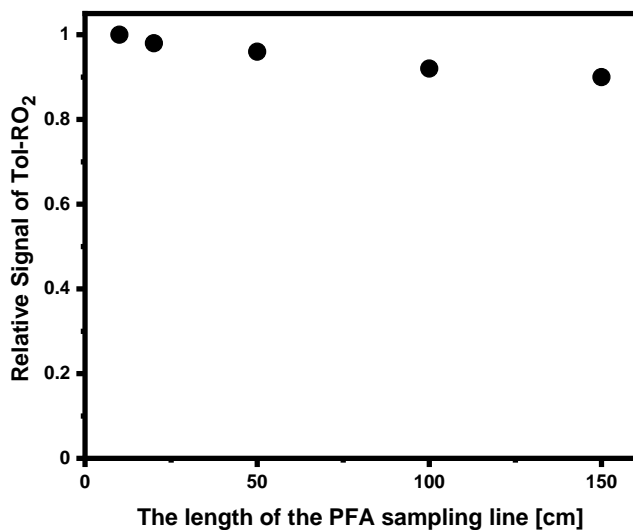
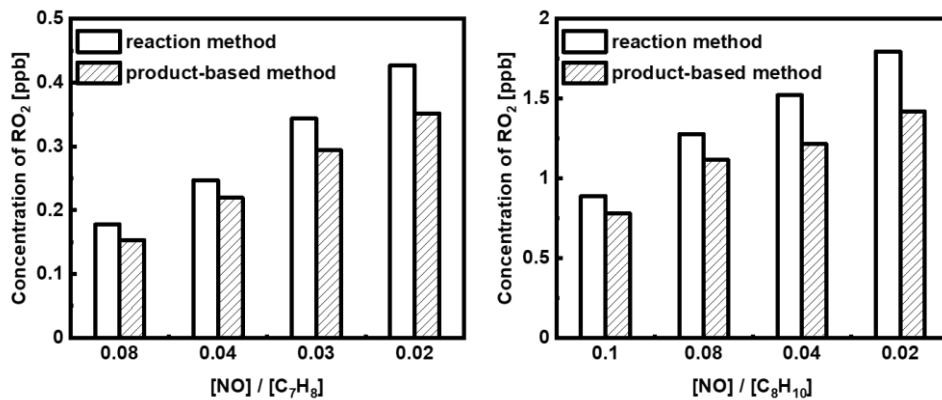


**Figure S6 Sampling loss assessment in PFA line (referenced to the signal at a line length of 0.1 m).**



65 Figure S7 Comparison of RO<sub>2</sub> concentration in the calibrated system estimated using two methods in the oxidation of (left) toluene and (right) m-xylene.

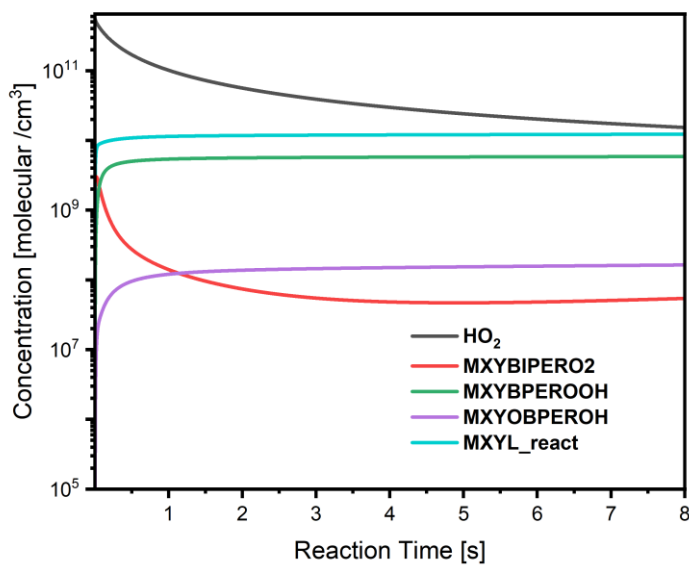
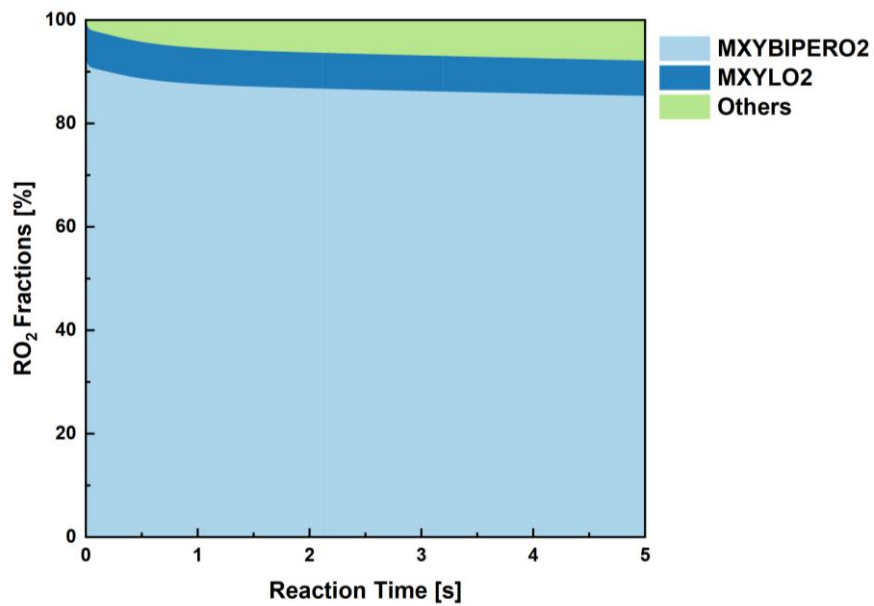


Figure S8 Temporal evolution of selected species according to the calibration flow tube kinetic model.



70

Figure S9 The fraction of RO<sub>2</sub> radicals according to the calibration flow tube kinetic model.

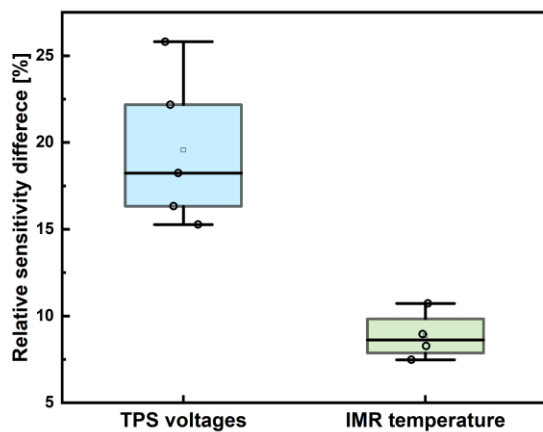


Figure S10 Sensitivity comparison between chosen and proxy-optimal conditions.